Steady-State Toroidal Plasma around a Spherical Anode in a Magnetic Field

R. G. Greaves, D. A. Boyd, J. A. Antoniades, and R. F. Ellis

Laboratory for Plasma Research, University of Maryland, College Park, Maryland 20742

(Received 8 November 1989)

When a positive potential is applied to a spherical electrode in the presence of a low-pressure gas in a uniform magnetic field, a stable toroidal plasma can form around the anode. This plasma is produced by electrons which are trapped in the combined electric and magnetic fields. We present observations of some of the basic properties of this plasma as measured using electrostatic probes and a low-light-level camera. We interpret these measurements in terms of an extended treatment of electromagnetic "bottles" which have been predicted to exist in this system.

When a positive potential is applied to a spherical anode in the presence of a weak magnetic field, a discharge can form at pressures below the Paschen curve. The plasma results from an ionization avalanche produced by trapped electrons.[1] Alport *et al.*[2] have shown that these plasmas can take one of two forms, which differ markedly from each other in their topology and electrical characteristics. For a given magnetic field and gas pressure, there is a characteristic anode potential below which an equilibrium toroidal plasma forms around the anode. The anode current in this case is relatively small, and is limited by the properties of the plasma rather than resistors in the external circuit. This phenomenon is of interest both in laboratory plasmas, where it relates to Langmuir-probe characteristics, and in space where it has a bearing on high-voltage systems being currently investigated.[3,4] At high anode potentials a higher-current spherical discharge is observed.

The toroidal plasma consists mainly of electrons moving in trapped orbits encircling the anode.[5] The magnetic field is too weak to affect appreciably the ion trajectories. In our system where the presence of the neutral gas cannot be neglected, trapping is important because it can lead to ionization.

Electrons moving in a uniform magnetic field, $B \| z$, around a spherical anode are dynamically confined within electromagnetic "bottles"[6] with boundaries given by

$$E = -e\phi(r,z) + \tfrac{1}{2} mr^2 \left[\frac{J}{mr^2} - \frac{\omega}{2} \right]^2 , \qquad (1)$$

where $\omega_c = eB/m$, $J = m\omega_c r_0^2$, $\phi(r,z)$ is the space potential, E is the electron energy, and r_0 is the radius of the field line which the electron is on at $z = \infty$. If the boundaries do not intersect the anode, the electrons ideally are permanently trapped. The trapped electrons follow complicated orbits within the bottles, and can gain sufficient energy to ionize neutral gas atoms with which they collide. In this Letter we show how the toroidal plasma we observe is related to these electromagnetic bottles.

The shape of the bottles depends on the form of the

space potential $\phi(r,z)$. For the space potentials we measure, the boundaries take one of two forms, depending on the value of E, as shown in Fig. 1: (i) For small values of $|E|$ (i.e., for electrons released far from the anode), two coaxial surfaces exist, between which the electrons are trapped. (ii) For larger values of $|E|$ (i.e., for electrons released by ionizing collisions), closed toroidal surfaces apply. These closed surfaces were not apparent in previous treatments since ionization was neglected. The bottles shown in Fig. 1 were computed subject to the condition that their minimum radius be equal to the anode radius. These bottles are of particular importance because they represent the innermost bottles where trapping can occur.

For $z \gg r_a$, the anode radius, both the inner and outer surfaces converge on a cylinder of radius r_{PM}, the Parker-Murphy radius,[6] given by

$$\frac{r_{PM}^2}{r_a^2} = 1 + \left[\frac{8e\phi_a}{m\omega_c^2 r_a^2} \right]^{1/2} , \qquad (2)$$

where ϕ_a is the anode potential. Note that this quantity is independent of the form of $\phi(r,z)$.

The experiment was performed in a cylindrical stainless-steel vessel 1.8 m in diameter and 4 m long. An axial magnetic field ($0 < B < 30$ G, $B \| z$) is produced by three magnetic field coils coaxial with the main axis of
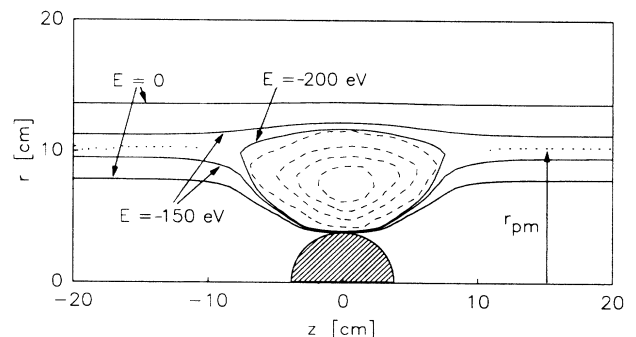

FIG. 1. Solid lines: electromagnetic bottles for $r_0 = r_{PM}$; dashed lines: contours of local intensity of light emission obtained by Abel inversion of low-light-level video images. $B = 15$ G, $\phi_a = 3$ kV, $p = 1.0 \times 10^{-4}$ Torr.

the vessel. The plasma was produced by applying a potential of typically 1-3 kV to a spherical anode 7.6 cm in diameter, mounted on the axis of the device. Formation of the toroidal plasma occurs only if the pressure, magnetic field, and anode potential are within certain critical ranges. Typical parameters were $B \sim 1\text{-}30$ G, $\phi_a \sim 1\text{-}5$ kV, and $p \sim (3\text{-}10) \times 10^{-5}$ Torr. The anode current I_a was typically 1-20 mA.

Light emission from the plasma is dominantly from a toroidal volume encircling the anode, with its major axis parallel to the magnetic field. This volume is separated from the anode by a dark space [Fig. 2(a)]. The structure of the luminous region can be seen more clearly when viewed radially, as shown in Figs. 2(b) and 2(c). The luminous region is roughly circular in cross section at low B field [Fig. 2(b)] but becomes elongated in the magnetic field direction as B is increased. For suf-

ficiently high values of B, in addition to the toroidal luminosity, a thin cylindrical shell extending the entire length of the chamber becomes visible [Fig. 2(c)]. Under these conditions, the plasma bears a strong resemblance to the bottles shown in Fig. 1.

Plasma properties were measured using collecting and emitting Langmuir probes and a retarding-potential energy analyzer. The radius of the probes and the probe stems were chosen so that the perturbation to the anode current was minimized. Typical perturbations were only a few percent. Radial potential profiles obtained using an emissive probe are illustrated in Fig. 3 for $B = 5$ and 15 G, together with the vacuum potential. The presence of the plasma considerably modifies the potential around the anode. The two-dimensional space potential $\phi(r,z)$ was measured with an emissive probe which could be moved both radially and axially. A typical potential map is shown in Fig. 4(a). From such data, the net charge density can be obtained using Poisson's equation, $\nabla^2 \phi = -\rho/\epsilon_0$. This is shown in Fig. 4(b) for the $z = 0$ radial section from Fig. 4(a). This profile shows electron-rich regions close to the anode surface, and at $r \sim 12$ cm, an ion-rich region. The sharply rising part of the curve on the left is due to positive charge on the surface of the sphere.

The ions are not magnetized but are accelerated almost radially outward from the ionization region to the chamber wall. On striking the chamber wall they eject secondary electrons, some of which contribute to the anode current. The ion energy spectrum was measured using a retarding-potential energy analyzer. Typical spectra for $\phi_a \sim 1$ kV display a broad peak at ~ 250 eV. This shows that most ionization occurs at a radial distance where $\phi(r) \sim 250$ V and this corresponds roughly to the ion-rich region in Fig. 4(b).

Accurate measurements of the electron density using Langmuir probes are problematic due to the presence of energetic electrons which can cause secondary-electron emission from the probe. However, order-of-magnitude estimates of density can be obtained by measuring the
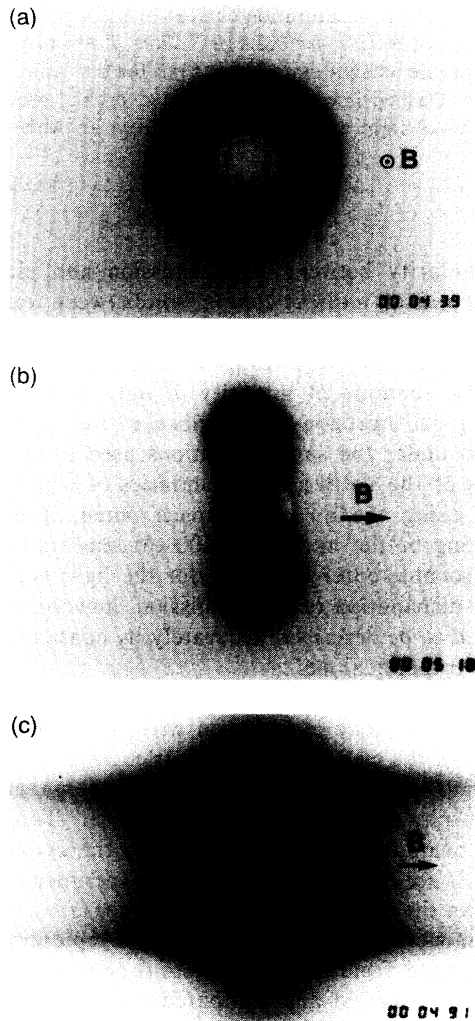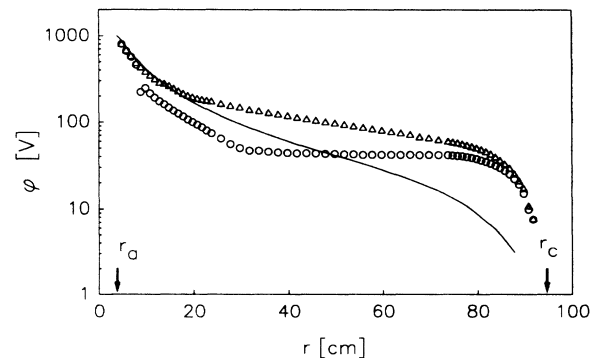

FIG. 2. Negative image of the toroidal plasma $p = 6 \times 10^{-5}$ Torr. (a) Axial view and (b) radial view for $\phi_a = 3$ kV, $B = 10$ G. (c) Radial view for $\phi_a = 5$ kV, $B = 30$ G.

FIG. 3. Radial potential profile for $\phi_a = 1$ kV, $p = 5.4 \times 10^{-5}$ Torr. (O) $B = 15$ G; ($\triangle$) $B = 5$ G. Solid line: the vacuum potential. r_c is the cathode radius.
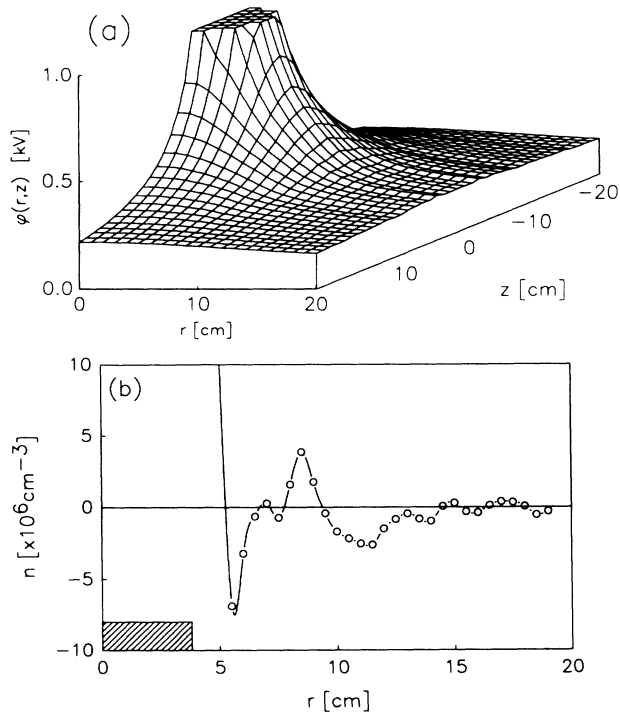
887

FIG. 4. (a) Space potential around the anode for $B = 12$ G, $p = 6.1 \times 10^{-5}$ Torr, $\phi_a = 1$ kV. (b) Net electric charge-density profile for $z = 0$ deduced from (a). The hatched area marks the anode radius.

FIG. 5. (a) Electron saturation current to a Langmuir probe with $B = 15$ G, $\phi_a = 1$ kV, $p = 9.2 \times 10^{-5}$ Torr, $I_a = 1$ mA, $z = 0$. (b) Radial profile of light emission at $z = 0$ for the same conditions as (a). Dashed line: chord-integrated profile; solid line: local intensity of light emission obtained from an Abel inversion.

collected electron current to a probe biased close to the plasma potential which is independently measured using a nearby emissive probe. This technique has allowed us to measure approximately the electron-density profile and to correlate it with the intensity of light emission. The results for typical conditions are shown in Fig. 5(a) where the electron current is plotted as a function of radial probe position.

The scale on the right of this figure indicates the nominal electron density, calculated using an effective electron energy of 50 eV estimated from the electron-retarding region of the probe characteristics. For comparison, the spatial light emission from the same plasma is shown in Fig. 5(b). This was obtained by recording an image of the plasma perpendicular to the z direction [such as Figs. 2(b) or 2(c)] using a low-light-level video camera. This represents the chord-integrated light emission. Since the plasma is cylindrically symmetrical about the z axis, a simple Abel inversion could then be performed on radial sections of the image to obtain the spatial distribution of the light emission. Data for the radial section through $z = 0$ are shown in Fig. 5(b). Note that the light emission and electron density peak at roughly the same radial position and have similar profiles. We do not expect exact agreement in this experiment since the light emission depends not only on the electron density but also on the electron energy spectrum (through the excitation cross section) which varies with
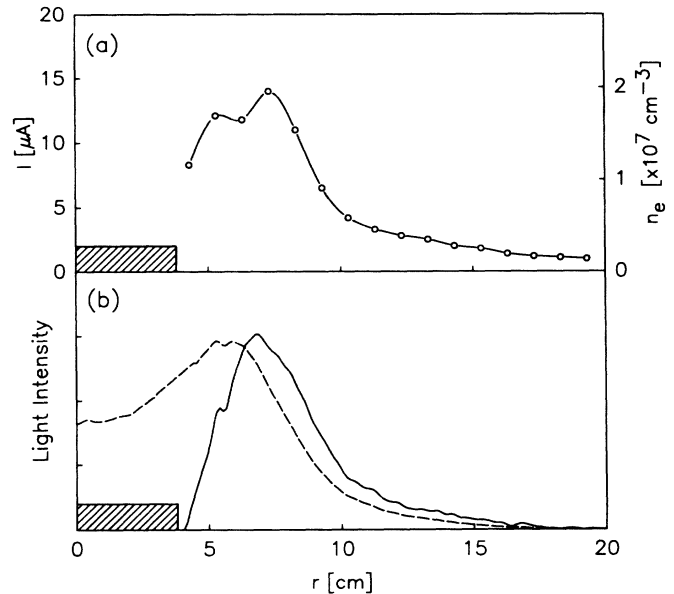
r.

This similarity between light emission and electron density permits an indirect comparison between the electrons and the shape of the electromagnetic bottles where we expect electrons to be trapped. The dashed lines in Fig. 1 show contours of intensity of light emission obtained by Abel inversion as described above. The data were taken under the same conditions used to compute the shapes of the bottles, the boundaries of which were computed using the measured space potential $\phi(r,z)$. The "grazing bottle" for $E = -200$ eV appears to provide a reasonable outer boundary for the light emission. The exact distribution of light emission, however, is too complicated to be described accurately by considerations of particle trapping alone.

There is, however, a feature of the discharge which permits a quantitative comparison with theory, namely, the portion of the electromagnetic bottles for $z \gg r_a$. For increasing values of E, these bottles converge on the Parker-Murphy radius, as shown in Fig. 1. This configuration bears a strong resemblance to the cylindrical shells which are often observed in the experiment. Figure 6 shows the radius of these shells measured over a range of anode potentials. The solid line represents the values computed from Eq. (2). There is good agreement between the measured and computed radii. This result appears to be the first direct observation of the Parker-Murphy radius in a ground-based experiment, although indirect evidence of its existence has been observed recently in the ionosphere.[7]
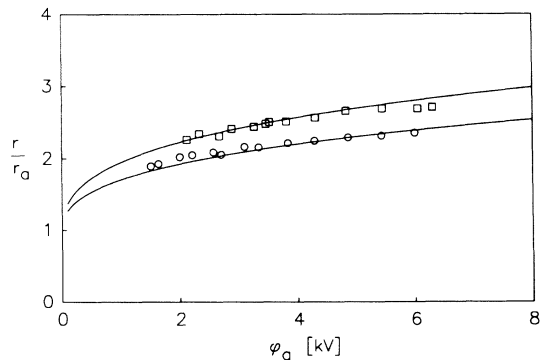
FIG. 6. Radius of maximum light intensity in the cylindrical section of the plasma. (O) $B=20$ G; (□) $B=30$ G. The solid lines were obtained from Eq. (2).

The phenomenon described here represents a well-defined plasma state existing in a sharply delineated region of the (p,B,ϕ_a) parameter space. An interesting feature of this plasma is the robust nature of the equilibrium. Such an equilibrium requires that there be an exact balance between the transport of trapped electrons to the anode and the introduction of electrons into the plasma by ionizing collisions and secondaries from the chamber wall. This balance is surprising in view of the exponential nature of the ionization avalanches which produce most of the electrons collected by the anode. The system is further complicated by the fact that the density is sufficiently high to perturb the space potential, which in turn influences the particle dynamics. The equilibrium must therefore also possess self-consistency between the fields and the particles.

One mechanism which could help to establish this equilibrium involves fluctuation-induced electron transport to the anode. We speculate that this could untrap electrons from the electromagnetic bottles and permit them to be collected by the anode without making inelas-tic collisions which would otherwise be necessary for them to leave the plasma. This would have a quenching effect on the cascade by providing a negative feedback mechanism.

Discharges of this type are of relevance to high-voltage experiments in space such as the SPEAR (Space Power Experiments Aboard Rockets) series of sounding rocket payloads[3] and the scheduled shuttle electro-dynamic tether mission.[4] The occurrence of such discharges could also account for the anomalously low satellite potentials attained during electron-beam emission in low Earth orbit.[8]

Note added.—Sasaki et al.[9] reported enhanced current collection by a spherical anode in a magnetoplasma due to ionization by trapped electrons associated with a luminosity encircling the anode.

[1]P. A. Redhead, Can. J. Phys. 36, 255 (1958); E. E. Kunhardt et al., in Proceedings of the Thirteenth International Symposium on Discharges and Electrical Insulation in Vacuum, Paris, 1988, edited by J. M. Buzzi and A. Settier (Les Editiones de Physique, Les Ulis, France, 1988), pp. 247–249.

[2]M. A. Alport et al., J. Geophys. Res. (to be published).

[3]D. B. Allred et al., IEEE Trans. Nucl. Sci. 35, 1386–1393 (1988).

[4]C. Bonifazi, Adv. Astronaut. Sci. 62, 173 (1987).

[5]P. Palmedesso (to be published).

[6]L. W. Parker and B. L. Murphy, J. Geophys. Res. 72, 1631 (1967); J. Rubinstein and J. G. Laframboise, Phys. Fluids 25, 1174–1182 (1982).

[7]N. B. Myers et al., Geophys. Res. Lett. 16, 365 (1989).

[8]I. Katz et al., J. Geophys. Res. 94, 1450 (1989).

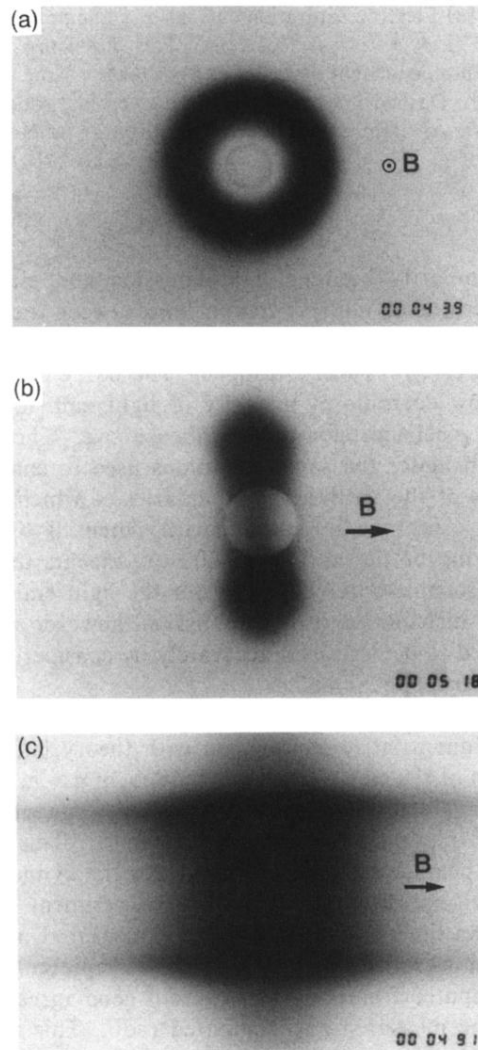[9]S. Sasaki et al., J. Geomag. Geoelectr. 36, 565 (1984).

FIG. 2. Negative image of the toroidal plasma $p = 6 \times 10^{-5}$ Torr. (a) Axial view and (b) radial view for $\phi_a = 3$ kV, $B = 10$ G. (c) Radial view for $\phi_a = 5$ kV, $B = 30$ G.